Stable Organic Radical for Enhancing Metal-Monolayer-Semiconductor Junction Performance

J. Alejandro de Sousa, Raphael Pfattner, Diego Gutiérrez, Kilian Jutglar, Stefan T. Bromley, Jaume Veciana, Concepcio Rovira, Marta Mas-Torrent, Bruno Fabre, Nuria Crivillers

Stable Organic Radical for Enhancing Metal-Monolayer-Semiconductor Junctions Performance

Jesús Alejandro De Sousa,[a,b] Raphael Pfattner,[a] Diego Gutiérrez,[a,†] Kilian Jutglar,[c] Stefan. T. Bromley,[c,d] Jaume Veciana,[a] Concepció Rovira,[a] Marta Mas-Torrent,[a] Bruno Fabre,[e] Núria Crivillers[a]*

[a] *Institut de Ciència de Materials de Barcelona (ICMAB, CSIC), Campus de la UAB s/n, Bellaterra, 081093, Spain*

[b] *Laboratorio de Electroquímica, Departamento de Química, Facultad de Ciencias, Universidad de los Andes, 5101 Mérida, Venezuela*

[c] *Departament de Ciència de Materials i Química Física & Institut de Química Teòrica i Computacional (IQTC), Universitat de Barcelona, c/ Martí i Franquès 1-11, 08028 Barcelona, Spain.*

[d] *Institució Catalana de Recerca i Estudis Avançats (ICREA), E-08010 Barcelona, Spain*

[e] *Univ Rennes, CNRS, ISCR (Institut des Sciences Chimiques de Rennes)-UMR 6226, F-35000* Rennes, France.

[†] Present address: Leitat Technological Center (LEITAT), Carrer Innovació, 2, 08225 Terrassa, Spain.

KEYWORDS

Organic radicals, charge transport, liquid metal, molecular junctions, silicon functionalization, photodiode.

ABSTRACT

The preparation of monolayers based on an organic radical and its diamagnetic counterpart has been pursued on hydrogen-terminated silicon surfaces. The functional monolayers have been investigated as solid-state Metal/monolayer/Semiconductor (MmS) junctions showing a characteristic diode behavior which is tuned by the electronic characteristics of the organic molecule. A Eutectic Gallium-Indium liquid metal is used as a top electrode to perform the transport measurements and the results clearly indicate that the presence of the SOMO-SUMO molecular orbitals impacts on the device performance. The junction incorporating the radical shows an almost two orders of magnitude higher rectification ratio (R ($|J_{1V}/J_{-1V}|$) = $10^{4.04}$) in comparison with the non-radical one (R ($|J_{1V}/J_{-1V}|$) = $10^{2.30}$). Interestingly, the high stability of the fabricated MmS permits to interrogate the system under irradiation, evidencing that at the wavelength where the photon energy is close to the band gap of the radical, there is a clear enhancement of the photo response. This is translated in an increase of the photo sensitivity (S_{ph}) value from 68.7 mA/W to 269.0 mA/W for the non-radical and radical, respectively.

INTRODUCTION

The use of organic molecules in electronics is nowadays one of the most promising approaches to develop devices displaying novel and tunable (opto)electronic properties based on the intrinsic molecular characteristics. From one side, organic molecules are already applied in streamline technologies such as OLEDs (organic light-emitting diodes) displays,[1] OFETs (organic field-effect transistors),[2,3] or flexible OPVs (organic photovoltaic) cells.[4] Although molecular-

scale electronics is still at an early stage of development for practical applications, the field has enormously grown in the past years. A significantly improved understanding of the molecule/electrode interfaces, charge transport mechanisms and molecular structure/device performance relationship, has been reached. Such in-depth comprehension level has permitted to widen the complexity of the investigated molecules towards the fabrication of functional molecular junctions (MJ).[5] Commonly, MJs are fabricated sandwiching a single molecule or an assembly of molecules between two metal electrodes. Interestingly, also the chemical functionalization of semiconducting substrates, like silicon (Si), has recently attracted attention due to its relevant technological interest.[6] The covalent functionalization of Si with organic molecules has opened up the possibility of tuning the electrical properties of the semiconductor beneath,[6,7] as well as of introducing additional functionalities such as redox activity[8] and bio-receptors.[9] Thus, the charge transport through solid-state Metal/monolayer/Semiconductor (MmS) junctions is of relevant interest. However, most of the research done so far on MmS is limited to alkyl molecular monolayers, and very few examples on small conjugated molecules can be found in literature.[10] Several parameters such as the molecular dipole, semiconductor dopant type and density, metal electrode characteristics or even the monolayer quality, have a strong impact on the energy level alignment, interface states and charge rearrangement. For this, in order to understand their effects on the electrical properties and thus, the (photo)device performance,[11] it is important to consider and control these different aspects.

Mercury has been widely used as metal contact for the fabrication and electrical characterization of large area MJ thanks to its mild top contact with the organic materials, resulting in the formation of metal or semiconductor/molecule/Hg junctions.[5] More recently, the eutectic gallium-indium alloy (EGaIn) has been successfully exploited as a less toxic alternative top contact

electrode[12,13] for studying the charge transport through organic monolayers assembled on metallic surfaces,[14] oxides[15] and, for the fabrication of other types of devices, like memories.[16,17] The EGaIn is a low-viscosity liquid at room temperature, it possesses unique properties and has a spontaneously formed thin oxide skin providing a non-Newtonian character. This enables intrinsic flexibility and stretchability combined with high electrical and thermal conductivity, while maintaining the possibility of shaping the EGaIn electrode as a contact tip.[18] The thickness of the GaO_x, spontaneously formed in air, was reported to be about 0.7 nm[19] with a typical resistivity of about 4.71 kΩ·cm, which is attributed to the presence of oxygen vacancies in the defective GaO_x thin layer.[20–22] This stays in sharp contrast to pure Ga_2O_3 (deposited by electron beam evaporation), which is a wide band gap semiconductor (E_g = 4.8 eV), and exhibits a large electrical resistivity of about 10^{12} - 10^{13} Ω·cm.[22] Thus, generally, in a molecular junction, the thin oxide layer contributes with a negligible resistance to the total molecular junction.

Among the large amount of families of molecules investigated in MJs, stable free organic radicals have gained an increasing attention over the last years.[23,24] Thanks to their open-shell electronic configuration, these molecules are paramagnetic and redox and optically active, which make them appealing species for a variety of applications.[25,26] Chlorinated trityl radicals, and in particular the perchlorotriphenylmethyl radicals (rad-PTMs), have shown to be highly stable as active molecular units in molecular junctions.[27–29] The comparison between junctions incorporating the open-shell (radical) or the closed-shell (non-radical) derivatives has permitted to unravel the role of the SOMO-SUMO orbitals (singly occupied molecular orbital-single unoccupied molecular orbital) in the transport mechanisms.[27,30] From temperature- and chain length-dependent measurements, it was corroborated that the mechanism of charge transport

across the junctions (EGaIn/PTM-monolayer/Au) was direct tunneling and that the SUMO of the radical participated in the transport, effectively lowering the tunneling barrier height.[27]

Recently, H-terminated *p*-type silicon (Si-H) was chemically modified through a hydrosilylation route with a PTM radical derivative bearing a terminal alkyne group. Such systems were demonstrated to work as a reversible electrochemical capacitive switch with good stability.[31] Herein, the charge transport of these systems, employing the open- and closed-shell molecules (**Rad-PTM** and **αH-PTM**, Figure 1a), is investigated. The monolayers were top-contacted with an EGaIn electrode, leading to a typical MmS junction. Both investigated junctions, *i.e.* radical and non-radical (αH), showed an expected Schottky-diode behavior for a metal/monolayer/semiconductor junction (i.e. current rectification) but, remarkably the radical-based MmS displayed higher current density in forward bias, which is associated to a more favorable interface energy level alignment due to the presence of the SOMO-SUMO orbitals. At reverse bias, the monolayer contribution into the measured current is negligible. Further, this interface was evaluated under illumination showing good stability and evidencing a clear effect of the radical on the current-response of the junction. To the best of our knowledge, this is the first example of a functional stable organic radical monolayer exploited to modulate the charge transport in MmS Schottky junctions.

RESULTS AND DISCUSSION

Functionalization and characterization of Si–H surfaces

Rad-PTM (open-shell), αH-PTM (closed-shell) and 1-ethynyl-4-hexylbenzene (closed-shell reference sample (EHB)) (Figure 1a) were grafted onto SiO_2-free *p*-type Si(111)-H substrates

via a hydrosilylation reaction using the alkyne group, following our previously reported experimental procedure[31] (see Figure 1b for monolayer structures). Rad-PTM and αH-PTM were synthesized as previously described.[29] The three different functionalized surfaces were further characterized by ellipsometry, X-ray photoelectron spectroscopy (XPS) and electrochemistry. Ellipsometry measurements yielded monolayer thicknesses of 16.1 ± 0.5 Å, 21.0 ± 1.0 Å and 21.8 ± 1.0 Å for **Si/EHB**, **Si/αH-PTM** and **Si/rad-PTM**, respectively. Such values are in good agreement with the theoretical molecular lengths estimated to be about 14.9, 18.8 and 18.6 Å, respectively (see also Figure S2 in the Supporting Information). XPS analysis of the three modified surfaces revealed characteristic peaks from the Si substrate and from the C 1s and Cl 2p core levels of the attached molecules (Figures S4-S7). For **Si/EHB**, the high-resolution C 1s spectrum displayed a main component at 285.0 eV corresponding to unresolved contributions of C-C and C=C bonds (Figure S4). Additionally, the Si 2p spectrum did not show any significant oxidation of the underlying silicon surface, in agreement with a dense monolayer (Figure S7). The C 1s and Cl 2p spectra of **Si/αH-PTM** (Figure S5) and **Si/rad-PTM** (Figure S6) were comparable. Furthermore, the experimental area under the C-C (C=C and C alpha) and C-Cl peaks was perfectly consistent with the expected 1.1 (15 C-C vs 14 C-Cl bonds) ratio, 1.1 for the αH-PTM and 1.2 for the rad-PTM, supporting a successful monolayer grafting. Another experimental evidence that the PTM molecules were not altered after grafting was provided by the atomic concentrations of carbon and chlorine determined from the peak areas which were perfectly in agreement with the expected chemical composition, namely 2.2 (αH-PTM) and 2.1 (rad-PTM) against 2.1 (29 carbon vs 14 chlorine atoms). The grafting of sterically hindered bulky PTM introduced some unavoidable oxidation of the underlying silicon surface, as evidenced by the presence of a small peak at a binding energy of 103.0 eV attributable to silicon oxides.[32] Importantly for the comparison of the

electrical properties of the junctions, the Si-O/Si ratio was found to be very similar for both PTM derivatives (Figure S7).

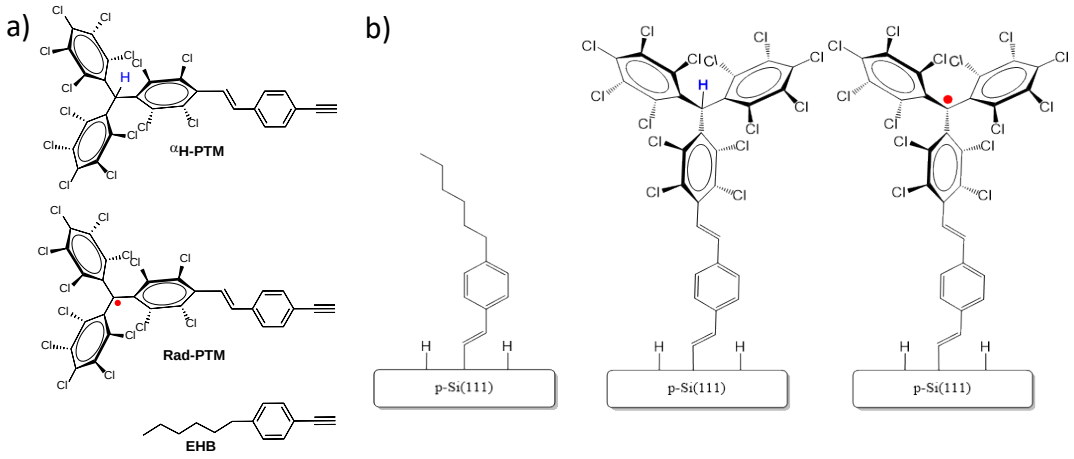

Figure 1. a) Chemical structure of the PTM derivatives (**αH-PTM** and **PTM-Rad**) and reference molecule (**EHB**) employed in this study. b) Scheme of the three molecular monolayer-modified Si(111) surfaces investigated in this work: **Si/EHB** (left), **Si/αH-PTM** (middle) and **Si/rad-PTM** (right).

The voltammetric analysis of the three modified surfaces, which was performed under illumination (100 mW cm^{-2}, AM 1.5G, SI) to activate the electron conduction of the Si substrate, revealed that only the **Si/rad-PTM** surface was electroactive (Figure S8). Indeed, the illuminated **Si/rad-PTM** showed a reversible redox wave corresponding to the PTM(radical)/PTM(anion) process, characterized by a non-ideal peak splitting. Such a double peak is believed to be originated from some lattice strain resulting from strong interactions between neighboring PTM units, as previously reported for ferrocenyl monolayers bound to gold.[33] Such a peak splitting is frequently observed for densely packed electroactive monolayers. Besides, the surface coverage of attached rad-PTM was estimated to be (7.5 ± 0.5) x 10^{-11} mol cm^{-2} from the integration of the anodic peak

photocurrent at different scan rates, which is relatively close to the value reported in our previous report, namely (8.5 ± 0.3) x 10^{-11} mol cm^{-2}.[31] Moreover, both anodic and cathodic peak photocurrent densities j_{pa} and j_{pc} were found to vary linearly with the scan rate (Figure S8-b), as expected for a surface-confined reversible redox species.[34]

To obtain further insights on the electronic properties of the modified surfaces, electrochemical impedance spectroscopy (EIS) measurements were performed. More particularly, the flatband potential V_{fb} of the silicon surface, i.e., the electrode potential for which there is no space charge region in the semiconductor, was estimated from the commonly used Mott-Schottky plot (C^{-2} vs V) that gives the space charge capacitance C_{sc} as a function of the electrode potential V under depletion conditions (i.e., depletion of valence band holes in the space charge region of the *p*-type surface). The calculated values of V_{fb} were in the range 0.26-0.30 V vs Saturated Calomel Electrode (SCE) and not significantly dependent on the nature of the immobilized molecule (Table S1 and Figure S9-S10). It is worth noticing that these values are very close to the ones extracted from solid-state capacitance measurements (*vide infra*).

Charge transport across Metal/Monolayer/Semiconductor (MmS) junctions

To perform charge transport measurements, the three different functionalized surfaces were soft top-contacted with a fresh EGaIn tip shaped as a cone exhibiting a typical geometrical contact area of about 900-1,600 μm^2. To avoid the influence of photogenerated carriers on the silicon substrate, all the measurements were performed in the dark. Twenty *J*-*V* traces were recorded applying a reverse bias followed by a forward bias employing a scan speed of 100 mV/s. All junctions were formed and measured with a freshly prepared tip in order to avoid variations in the oxide skin thickness and roughness over time.[35]

As shown in Figure 2, **Si/αH-PTM** and **Si/rad-PTM** junctions exhibit a clear diode behavior showing good reproducibility as well as a remarkable stability with a 100 % yield of the junctions formation (see Table S2 for the statistical data). Other junctions on silicon substrates were already reported to be very reliable, which was attributed to the C-Si bond stability and the smoothness of the silicon surface.[6,7] As expected for a diode, both junctions show rectification behavior but, remarkably, the **Si/rad-PTM**//GaOx/EGaIn shows almost two orders of magnitude higher rectification ratio $R|J_{1V}/J_{-1V}| = 10^{4.04}$ in comparison with the **Si/αH-PTM**//GaOx/EGaIn with a $R|J_{1V}/J_{-1V}| = 10^{2.30}$, this value being independent of the contact area (Figure S11). Generally, in molecular electronics, the current rectification depends on different factors such as the molecular structure[36,37] and the band/energy level alignment.[38,39] In the case of MmS junctions, the molecular conductivity, the Si-C-R dipole, the monolayer quality (i.e. presence of defects) and the monolayer/top contact interface can influence the energy levels alignment which impacts on the charge transport behaviour[6,7] thus, also on the rectification ratio.[40,41] Although it is well established that the presence of an interfacial dipole layer affects the depletion region (thus the Schottky barrier height), here, similar molecular dipoles are expected for the αH-PTM and the rad-PTM.[42] Importantly, the distinct rectification ratio is not attributed to the small differences in the content of surface silicon oxide seen by XPS because, such a different defect density is expected to have an influence at low applied bias where the Schottky barrier dominates the transport,[32] which is not the case here. On the contrary, in the high bias regime, where the measured current is dominated by the transport through the monolayer, i.e. when the molecular electronic structure plays a role, we do observe the influence of the molecules. As illustrated in the schematic energy band diagram of Figure 2b, it is clear that the Rad-PTM shows a lower SOMO/SUMO band gap compared to the HOMO/LUMO band gap of the αH -PTM. The SOMO/SUMO (-6.24 eV/-3.81 eV) and

HOMO/LUMO (-6.40 eV/-2.30 eV) energy values have been determined by DFT calculations (see SI), giving values similar to other reported systems.[30]

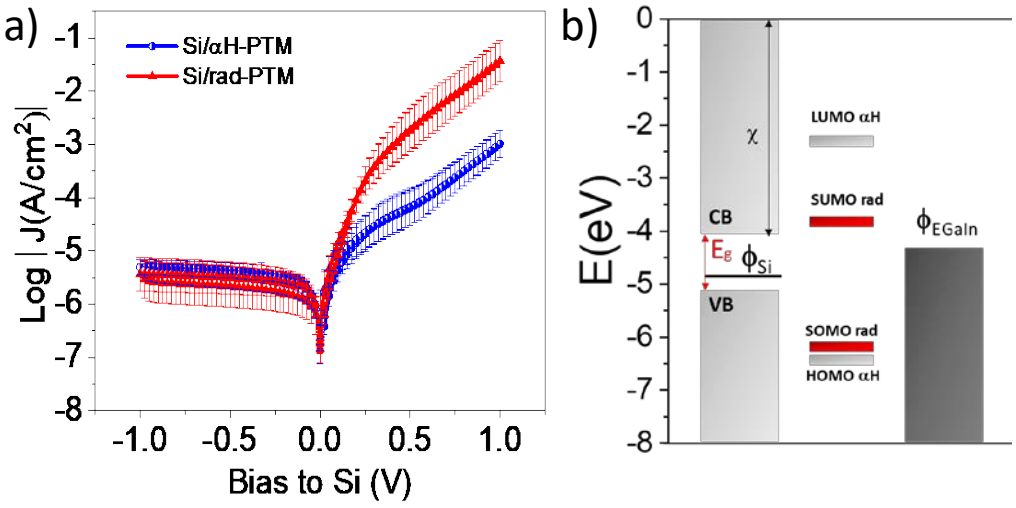

Figure 2. a) Semilog plot of *J* vs the voltage applied on Si (V) for **Si/PTM**//GaOx/EGaIn junctions: rad-PTM (red) and αH-PTM (blue), 20 junctions x 20 traces were measured. *b)* Scheme of the band diagram of the interfaces. This representation does not take into account changes in the electron affinity of silicon. E_g is the band gap energy of Si (1.12 eV)[43]; χ is the silicon electron affinity (4.05 eV)[43] and φ is the EGaIn work function (4.3 eV).[44]

From the *J-V* plots, it can be seen that at reverse bias, the current is negligible for both junctions and practically constant, as expected for an ideal diode behaviour in the off state. Remarkably, clear differences are observed at forward bias (i.e. with the diode in the on state). Indeed, the **Si/rad-PTM** surface displays an enhanced current density (by a factor of 35) in comparison with **Si/αH-PTM**. As previously mentioned in metal/radPTM/metal junctions, such a trend could be attributed to a decrease in the injection barrier due to the participation of the SUMO energy level

in the transport.[27,30] However, in MmS junctions, it must be kept in mind that a second barrier (i.e. a Schottky barrier) arises.

Hence, with the aim to determine the values of the barrier height and to get more insights on the charge transport mechanisms, solid-state impedance spectroscopy measurements (capacitance versus voltage) were carried out. Mott-Schottky analysis was performed to determine the flatband potential $|V_{fb}|$ which permits to identify different transport regimes. At reverse bias, when $|V_{bias}| < |V_{fb}|$, the charge transport is governed by the Schottky barrier and its magnitude is attenuated by the monolayer. While, at forward bias, when $|V_{bias}| > |V_{fb}|$, the charge transport is governed by the molecule characteristics and the transport is similar to a Metal/molecule/Metal junction. Thus, this zone allows comparing the charge transport through the molecules without the influence of the Schottky barrier.[7,43] Figure S12 shows the different schematic energy diagrams associated to these different voltages ranges.

Capacitance-voltage measurements and barrier height determination

To avoid discharging of the interface states during the determination of flat band potential, the capacitance was measured at 0.5 MHz and the amplitude of the AC signal was fixed at 50 mV.[6,43,45] To support our characterization and analysis approach, two additional junctions were examined as reference systems, namely the **Si/SiOx**//GaOx/EGaIn and the **Si/EHB**//GaOx/EGaIn (Figure 1 and Figure S17). The EHB layer was chosen since the linker unit (-Ph-C=C-Si) is the same compared to the PTM derivatives, but it is expected to form a more densely packed monolayer due to the absence of the bulky PTM moiety. Figure 3 shows representative Mott-Schottky plots (at 0.5 MHz) for the different interfaces. A typical behavior for a *p*-type semiconducting substrate is observed

with a clear change of the capacitance in the depletion region (~ 0-0.75 V). Extracted parameters are average values of three different *C*-*V* measurements (Figures S13-S16).

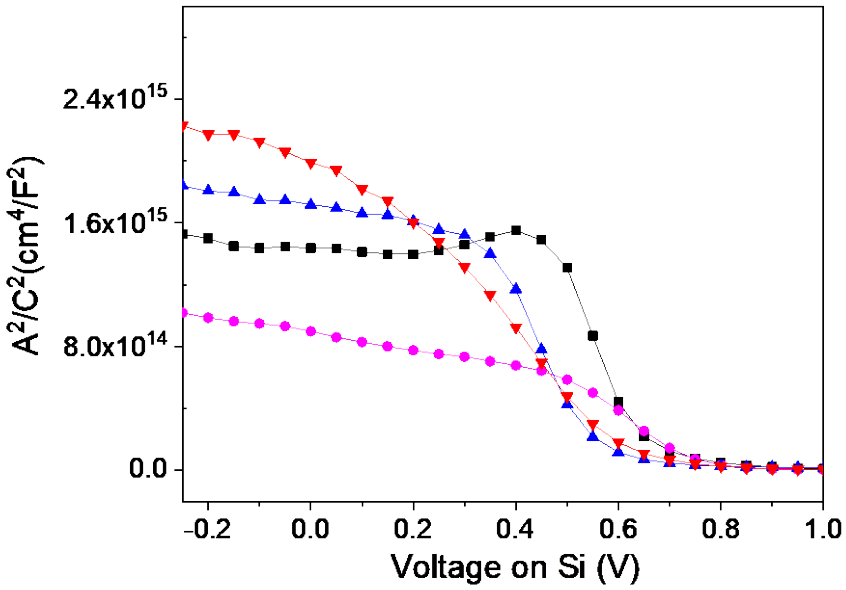

Figure 3. Capacitance-voltage measurements plotted as A^2/C^2 vs bias voltage for **Si/layer**//GaOx/EGaIn junctions with **layer** = **Rad-PTM** (red), **αH-PTM** (blue), **SiO_2** (black) and **EHB** (pink).

Table 1 summarizes the different parameters extracted by fitting the data to the Mott-Schottky model (Equation S2). As mentioned earlier, the obtained dopant density values are close to those determined by electrochemical measurements (Figure S10) and with the resistivity range provided by the supplier of the silicon wafers (in the range 5-15 Ω cm). Moreover, considering that the work function of EGaIn/GaO_x is ca. 4.3 eV vs the vacuum level[46] and assuming that the potential of SCE is -4.68 eV vs the vacuum energy,[47] the average V_{fb} values extracted from solid-state capacitance measurements can be estimated to 0.31 V, 0.37 V, 0.20 V and 0.23 V vs SCE for junctions integrating **Si/SiO_x**, **Si/EHB**, **Si/αH-PTM** and **Si/rad-PTM**, respectively. Overall, the

values obtained for molecular junctions agree relatively well with those determined from electrochemical measurements in solution.

Table 1. Transport parameters extracted from the impedance measurements of the different junctions: flatband potential $|V_{fb}|$, dopant density (N_D) and barrier height (ϕ_b). The values were extracted as an average of three distinct samples.

Junction	N_D***10**^{15}**(cm^{-3})**	**$\|V_{fb}$ (V)$\|$**	**ϕ_b (eV)**
Si/SiOx//GaOx/EGaIn	1.4 ± 0.1	0.69 ± 0.02	0.92 ± 0.02
Si/EHB//GaOx/EGaIn	5.5 ± 0.5	0.75 ± 0.04	0.94 ± 0.04
Si/αH-PTM//GaOx/EGaIn	1.9 ± 0.4	0.58 ± 0.01	0.80 ± 0.01
Si/rad-PTM//GaOx/EGaIn	2.5 ± 0.3	0.61 ± 0.03	0.82 ± 0.03

The interfacial MmS barrier height (ϕ_b) can be calculated with the above experimentally determined $|V_{fb}|$ and the N_D using Equations S5 and S6. The obtained values are given in Table 1. It is worth noticing that the experimental extracted ϕ_b value for the **Si/SiOx**//GaOx/EGaIn junction agrees quite well with the theoretical calculated value of 0.87 eV (for Si//EGaIn, see Section 5 in the SI). In order to check the validity of our approach, a complementary extraction method of $|V_{fb}|$ was done using Equation S9, obtaining $|V_{fb}| = 0.61 \pm 0.02$ V (see SI and Figure S15) which is in agreement with the theoretical value of 0.66 V. The PTMs and EHB monolayers have an influence on the depletion region decreasing and increasing the ϕ_b, respectively. Although the influence of the monolayer quality effect cannot completely be discarded,[7,32] the observed differences can be associated to the different interfacial dipoles,[6,40,41] which are expected to be different for the alkyl terminated layer versus the chlorinated phenyl rings of the PTM moiety.

***J*-*V* curves analysis**

To get information on the mechanism governing the PTM-based junctions investigated in this work, we have analyzed in depth the current density-voltage *J*-*V* curves. At forward bias below the flatband voltage ($0 < |V_{bias}| < |V_{fb}|$), i.e. when most of the bias voltage drops across the semiconductor depletion region, the most likely charge transport mechanisms in this situation are thermionic emission, minority carrier diffusion and generation recombination.[48,49] The ideality factor (*n*) and the effective Schottky barrier height (ϕ_{eff}), which take into consideration the attenuation caused by the monolayer to the transport, can be obtained by fitting the data to the ideal diode equation (Equation S11, see Section 6 in the SI). Thus, these values are used to determine the mechanism responsible for the charge transport. It is important to mention that Equation S11 is valid at low forward bias when the total resistance of the device is negligible.[49,50]

Following this approach, ideality factors of $n = 1.4 \pm 0.1$ and $n = 1.3 \pm 0.1$ were determined for **Si/αH-PTM**//GaOx/EGaIn and **Si/rad-PTM**//GaOx/EGaIn, respectively (Figure S16). Values of $n = 1$ are expected for ideal thermionic emission. Irregularities within the monolayer could increase the fitted *n* and lower ϕ_{eff} (*J*-*V*). Equal ϕ_{eff} were found for both interfaces, ϕ_{eff} (**Si/αH-PTM**) = 0.74 ± 0.01 eV and ϕ_{eff} (**Si/rad-PTM**) = 0.74 ± 0.01 eV. The fact of having an ϕ_{eff}(*J*-*V*)<ϕ_b(*C*-*V*), suggests an inhomogeneous barrier, which could be rationalized by the influence of some monolayer defects.[49,50]

In view of all the relevant values obtained from the experimental data and taking into consideration the similarity between both PTM-based monolayers in terms of: intrinsic dipole (almost equal Schottky barrier ϕ_b), monolayer packing and thickness (similar tunneling distance) and same measurement conditions, the only way to rationalize the significant current density enhancement at forward bias in the case of the open-shell interface, is the presence of the SOMO/SUMO orbitals. Thus, the energetic proximity of the molecular orbitals with the injection electrode decreases the tunneling barrier leading to an increase of the resulting measured current. An energetic diagram of the interfaces is proposed in Figure 2b. As mentioned above, this phenomenon was already previously observed for MomM interfaces.[27,30] Remarkably, this interpretation is reinforced when $|V_{bias}| > |V_{fb}|$, *i.e.* under accumulation, wherein the charge transport is controlled by the tunneling transport through the monolayer[51–53] and, the difference in J is more pronounced. In this bias regime, the interface behavior resembles a MmM device.

Photoresponse behavior of the junctions

To go a step further on the function evaluation, the photoresponse of the junctions was inspected. Thereby, charge transport measurements under different red laser intensities were performed (λ = 635 nm, photon energy E_{ph} = 1.95 eV) which is very close to the PTM radical SUMO-SOMO bandgap[30,54] (see Figure S1 for a scheme of the experimental setup used). Further, this wavelength does not promote the radical decomposition and is lower than the HOMO/LUMO gap of the αH-PTM. Figures 4a and 4b show the *J*-*V* curves at different irradiation powers for **Si/αH-PTM**//GaOx/EGaIn and **Si/rad-PTM**//GaOx/EgaIn, respectively. Clearly, for both systems, the photocurrent increases as a function of the laser intensity due to the photogenerated charge carriers (see Figure S20 for the band diagram changes upon illumination). The open-circuit voltage $|V_{OC}|$ (Figure 4c) increases exponentially with the laser power density, which was previously also

reported for organic solar cells.[55] The short-circuit current density $|J_{SC}|$ increases linearly with the irradiation intensity (Figure 4d), in agreement with the expected typical photodiode characteristics for both junctions.[11,56,57] Interestingly, the photosensitivity (S_{ph}) for the rad-PTM is four times higher compared to the **Si/αH-PTM**, being about 269.0 mA/W against 68.7 mA/W.

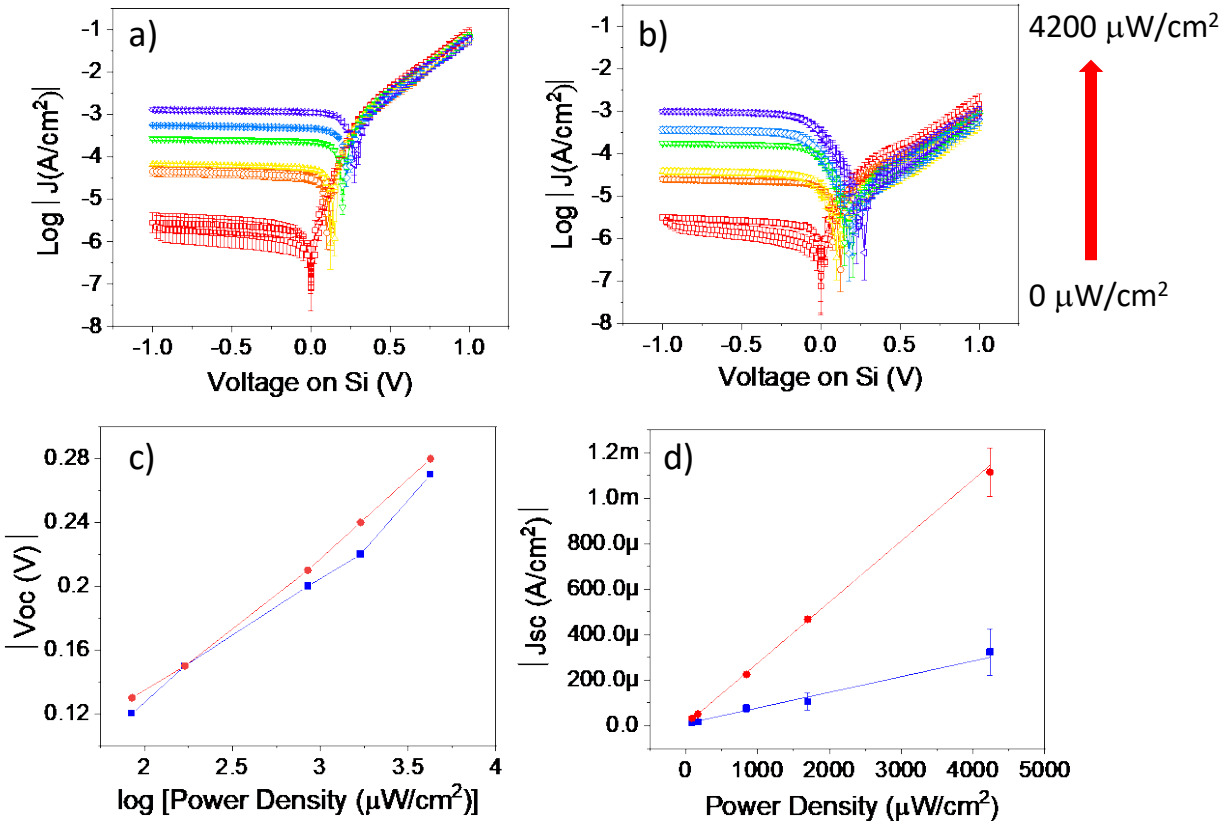

Figure 4. *J-V* measurements under different irradiation powers across a) **Si/rad-PTM** and b) **Si/αH-PTM**. c) Open circuit voltage V_{oc} and d) short circuit current density J_{sc} of **Si/rad-PTM** (red) and **Si/αH-PTM** junctions (blue). The linear regressions using Equation S13 gave S_{ph}= 68.7 mA/W for **Si/αH-PTM** and S_{ph}= 269.0 mA/W for **Si/rad-PTM**, with R^2 = 0.96 and 0.99, respectively.

These results show an improvement of the photodiode properties by the incorporation of low-band gap molecules in the visible spectrum at the interface, as the organic radicals studied herein. Our results enlarge the potential use of these systems in photovoltaic devices.[58]

Finally, another very important aspect is the operation stability. This issue becomes especially relevant for future molecular junctions applications. The ON/OFF ratio values (illumination/dark) for the two monolayers were found to be ~376 and ~188, for **Si/rad-PTM** and **Si/αH-PTM**, respectively. Charge transport measurements were continuously measured for one hour, performing pulses of irradiation (6-8 sec), under 170 μW/cm^2 and operating the diode in photovoltaic mode (0 V of applied bias voltage). As depicted in Figure 5, the **Si/rad-PTM**-based junction was relatively stable in operation with a negligible loss in the photocurrent over 1 h, whereas a ~40 % loss was observed for the **Si/αH-PTM**-based junction. Figure S21 shows the full variation of *J* along the 3,600 consecutive cycles performed, showing the photoresponse trend for both monolayers. The origin of such a discrepancy between both interfaces is currently unclear. The difference in the J_{SC} magnitude (at 0 V) is in agreement with the above discussed charge transport measurements in the dark, where the SOMO/SUMO presence in the radical-PTM enhance the *J* values.

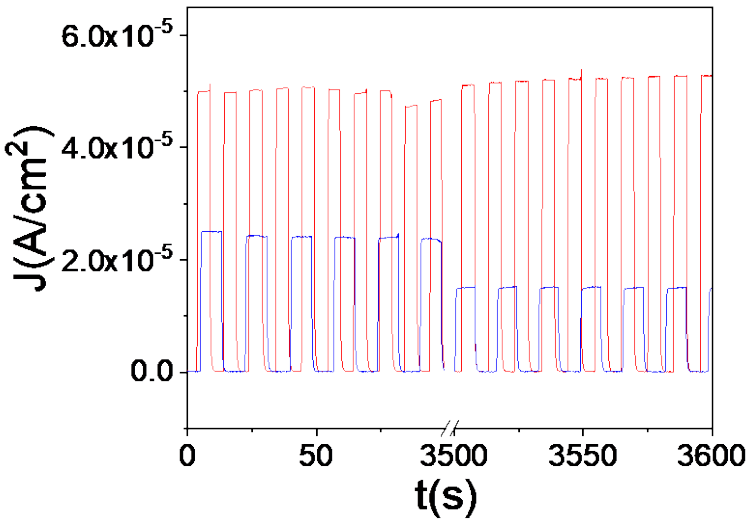

Figure 5. Stability of the junctions under 170 μW/cm^2 at 0 V bias voltage for 3,600 ON/OFF cycles of irradiation/dark: **Si/αH-PTM** (blue) and **Si/rad-PTM** (red).

CONCLUSIONS

In summary, we have demonstrated the successful incorporation of an open-shell molecule into a MmS structure (**Si/rad-PTM**//GaOx/EGaIn), displaying a diode behavior with higher rectification ratio with respect to the closed-shell counterpart. Impedance measurements were performed to analyze in depth the influence of the SOMO/SUMO orbitals into the interface electrical performance. It is demonstrated that the current density in the accumulation regime can be modulated by the incorporation of the radical that has a lower energy gap compared with the non-radical counterpart, improving the energy level alignment. Thus, these results support that the modification of Si with functional molecules is an appealing strategy to tune the Si-based junction properties. Additional length dependence studies could give the much-needed understanding on the charge transport mechanism, providing the basis for choosing novel systems with a pre-

designed junction functionality. In addition in this work, the photoresponse of the PTM-based MmS junctions has been investigated, showing a photosensitivity four-fold higher for the **Si/rad-PTM**//GaOx/EGaIn in comparison with the closed-shell organic layer. The junctions have shown a remarkable stability for over 3,600 on/off light irradiation cycles. Our findings can contribute to consolidate in a long-term vision, the use of such molecular systems into current silicon-based devices. In particular, they can pave the way for the preparation of photoresponsive switches wherein the photodiode behavior can be modulated by the intrinsic properties of the molecular system incorporated into the junction. Further, the stability of the radicals under irradiation endows to consolidate their use in other devices, like MmS solar cells, where the open-shell nature can participate and affect the device performance.

ASSOCIATED CONTENT

Supporting Information. The following files are available free of charge. Additional experimental details, materials, and methods, including schemes of experimental setup. Preparation and additional characterization of the monolayers (XPS, cyclic voltammetry and impedance spectroscopy measurements) and their corresponding junctions (diode junction characteristics and supporting electrical characterization).

AUTHOR INFORMATION

Corresponding Author

* **Núria Crivillers —** Institut de Ciència de Materials de Barcelona, ICMAB-CSIC, Campus UAB, 08193 Bellaterra, Spain. E-mail: ncrivillers@icmab.es

Present Addresses

† *Leitat Technological Center (LEITAT), Carrer Innovació, 2, 08225 Terrassa, Spain.*

Author Contributions

J.A.dS, R.P and N.C designed the experiments. J.A.dS and R.P performed the electrical characterization and light irradiation experiments and executed the data analysis. B.F prepared the monolayers covalently bound to H-terminated Si and performed their electrochemical characterization. D. G. and J.A.dS optimized the experimental set-up. K. J. and S. T. B performed the DFT calculations. All authors contributed to the results discussion. C.R., M.M-T and N.C conceived the project. N.C supervised the work. The manuscript was written through contributions of all authors. All authors have given approval to the final version of the manuscript.

ACKNOWLEDGMENT

This work was funded by MCIN/AEI/10.13039/501100011033 (grant GENESIS PID2019-111682RB-I00), the TED2021-122550B-C22, the "Severo Ochoa" Programme for Centers of Excellence in R&D FUNFUTURE CEX2019-000917-S and by the Generalitat de Catalunya (2017-SGR-918). The work was also supported by CSIC Interdisciplinary Thematic Platform (PTI+) on Quantum Technologies (PTI-QTEP+). This research is part of the CSIC program for the Spanish Recovery, Transformation and Resilience Plan funded by the Recovery and Resilience Facility of the European Union, established by the Regulation (EU) 2020/2094). This work was supported by the following research grants: PID2021-127957NB-I00 and TED2021-132550B-C21 (Ministerio de Ciencia e Innovación), CEX2021-001202-M ("María de Maeztu" program for Spanish Structures of Excellence). We also acknowledge access to supercomputer resources as

provided by the Red Española de Supercomputación. J.A.d S. is enrolled in the UAB Materials Science PhD program. R.P. acknowledges support from the Ramón y Cajal Fellowship (Ref. RyC2019-028474-I). S. Ababou-Girard and C. Meriadec (Institut de Physique de Rennes, UMR6251, France) are fully acknowledged for some XPS measurements on the Si–H surfaces.

REFERENCES

(1) Hong, G.; Gan, X.; Leonhardt, C.; Zhang, Z.; Seibert, J.; Busch, J. M.; Bräse, S. A Brief History of OLEDs—Emitter Development and Industry Milestones. *Adv. Mater.* **2021**, *33* 2005630- 2005654.

(2) Wang, Y.; Zhang, J.; Zhang, S.; Huang, J. OFET Chemical Sensors: Chemical Sensors Based on Ultrathin Organic Field-Effect Transistors. *Polym. Int.* **2021**, *70*, 414–425.

(3) Liu, K.; Ouyang, B.; Guo, X.; Guo, Y.; Liu, Y. Advances in Flexible Organic Field-Effect Transistors and Their Applications for Flexible Electronics. *npj Flex. Electron.* **2022**, *6, 1-19*.

(4) Fukuda, K.; Yu, K.; Someya, T. The Future of Flexible Organic Solar Cells. *Adv. Energy Mater.* **2020**, *10*, 2000765- 2000775.

(5) Jeong, H.; Kim, D.; Xiang, D.; Lee, T. High-Yield Functional Molecular Electronic Devices. *ACS Nano* **2017**, *11*, 6511–6548.

(6) Vilan, A.; Cahen, D. Chemical Modification of Semiconductor Surfaces for Molecular Electronics. *Chem. Rev.* **2017**, *117*, 4624–4666.

(7) Vilan, A.; Yaffe, O.; Biller, A.; Salomon, A.; Kahn, A.; Cahen, D. Molecules on Si: Electronics with Chemistry. *Adv. Mater.* **2010**, *22*, 140–159.

(8) Fabre, B. Functionalization of Oxide-Free Silicon Surfaces with Redox-Active Assemblies. *Chem. Rev.* **2016**, *116*, 4808–4849.

(9) Henriksson, A.; Neubauer, P.; Birkholz, M. Functionalization of Oxide-Free Silicon Surfaces for Biosensing Applications. *Adv. Mater. Interfaces.* **2021**, 8, 2100927-2100946.

(10) Haj-Yahia, A. E.; Yaffe, O.; Bendikov, T.; Cohen, H.; Feldman, Y.; Vilan, A.; Cahen, D. Substituent Variation Drives Metal/Monolayer/Semiconductor Junctions from Strongly Rectifying to Ohmic Behavior. *Adv. Mater.* **2013**, *25*, 702–706.

(11) Har-Lavan, R.; Ron, I.; Thieblemont, F.; Cahen, D. Toward Metal-Organic Insulator-Semiconductor Solar Cells, Based on Molecular Monolayer Self-Assembly on n-Si. *Appl. Phys. Lett.* **2009**, *94*, 043308.

(12) Reus, W. F.; Thuo, M. M.; Shapiro, N. D.; Nijhuis, C. A.; Whitesides, G. M. The SAM, Not the Electrodes, Dominates Charge Transport in Metal-Monolayer//Ga_2O_3/Gallium-Indium Eutectic Junctions. *ACS Nano* **2012**, *6*, 4806–4822.

(13) Nijhuis, C. A.; Reus, W. F.; Whitesides, G. M. Molecular Rectification in Metal - SAM - Metal Oxide - Metal Junctions. *J. Am. Chem. Soc.* **2009**, *131*, 17814–17827.

(14) Liu, Y.; Qiu, X.; Soni, S.; Chiechi, R. C. Charge Transport through Molecular Ensembles: Recent Progress in Molecular Electronics. *Chem. Phys. Rev.* **2021**, *2*, 021303.

(15) Lamport, Z. A.; Broadnax, A. D.; Scharmann, B.; Bradford, R. W.; Delacourt, A.; Meyer, N.; Li, H.; Geyer, S. M.; Thonhauser, T.; Welker, M. E.; Jurchescu, O. D. Molecular Rectifiers on Silicon: High Performance by Enhancing Top-Electrode/Molecule Coupling. *ACS Appl. Mater. Interfaces* **2019**, *11*, 18564–18570.
(16) Gutierrez, D.; de Sousa, J. A.; Mas-Torrent, M.; Crivillers, N. Resistive Switching Observation in a Gallium-Based Liquid Metal/Graphene Junction. *ACS Appl. Electron. Mater.* **2020**, *2*, 3093–3099.
(17) Almadhoun, M. N.; Speckbacher, M.; Olsen, B. C.; Luber, E. J.; Sayed, S. Y.; Tornow, M.; Buriak, J. M. Bipolar Resistive Switching in Junctions of Gallium Oxide and p-Type Silicon. *Nano Lett.* **2021**, *21*, 2666–2674.
(18) Nijhuis, C. A.; Reus, W. F.; Barber, J. R.; Whitesides, G. M. Comparison of SAM-Based Junctions with Ga_2O_3/EGaIn Top Electrodes to Other Large-Area Tunneling Junctions. *J. Phys. Chem. C* **2012**, *116*, 14139–14150.
(19) Chen, X.; Hu, H.; Trasobares, J.; Nijhuis, C. A. Rectification Ratio and Tunneling Decay Coefficient Depend on the Contact Geometry Revealed by in Situ Imaging of the Formation of EGaIn Junctions. *ACS Appl. Mater. Interfaces* **2019**, *11*, 21018–21029.
(20) Simeone, F. C.; Yoon, H. J.; Thuo, M. M.; Barber, J. R.; Smith, B.; Whitesides, G. M. Defining the Value of Injection Current and Effective Electrical Contact Area for Egain-Based Molecular Tunneling Junctions. *J. Am. Chem. Soc.* **2013**, *135*, 18131–18144.
(21) Suchand Sangeeth, C. S.; Wan, A.; Nijhuis, C. A. Probing the Nature and Resistance of the Molecule-Electrode Contact in SAM-Based Junctions. *Nanoscale* **2015**, *7*, 12061–12067.
(22) Sangeeth, C. S. S.; Wan, A.; Nijhuis, C. A. Equivalent Circuits of a Self-Assembled Monolayer-Based Tunnel Junction Determined by Impedance Spectroscopy. *J. Am. Chem. Soc.* **2014**, *136*, 11134–11144.
(23) Ratera, I.; Vidal-Gancedo, J.; Maspoch, D.; Bromley, S. T.; Crivillers, N.; Mas-Torrent, M. Perspectives for Polychlorinated Trityl Radicals. *J. Mater. Chem. C* **2021**, *9*, 10610–10623.
(24) Mas-Torrent, M.; Crivillers, N.; Rovira, C.; Veciana, J. Attaching Persistent Organic Free Radicals to Surfaces: How and Why. *Chem. Rev.* **2012**, *112*, 2506–2527.
(25) Chen, Z. X.; Li, Y.; Huang, F. Persistent and Stable Organic Radicals: Design, Synthesis, and Applications. *Chem* **2021**, *7*, 288–332.
(26) Mas-Torrent, M.; Crivillers, N.; Mugnaini, V.; Ratera, I.; Rovira, C.; Veciana, J. Organic Radicals on Surfaces: Towards Molecular Spintronics. *J. Mater. Chem.* **2009**, *19*, 1691–1695.
(27) Yuan, L.; Franco, C.; Crivillers, N.; Mas-Torrent, M.; Cao, L.; Sangeeth, C. S. S.; Rovira, C.; Veciana, J.; Nijhuis, C. A. Chemical Control over the Energy-Level Alignment in a Two-Terminal Junction. *Nat. Commun.* **2016**, *7*, 12066–12075.
(28) Frisenda, R.; Gaudenzi, R.; Franco, C.; Mas-Torrent, M.; Rovira, C.; Veciana, J.; Alcon, I.; Bromley, S. T.; Burzurí, E.; Van Der Zant, H. S. J. Kondo Effect in a Neutral and Stable All Organic Radical Single Molecule Break Junction. *Nano Lett.* **2015**, *15*, 3109–3114.
(29) Bejarano, F.; Olavarria-Contreras, I. J.; Droghetti, A.; Rungger, I.; Rudnev, A.; Gutiérrez, D.; Mas-Torrent, M.; Veciana, J.; Van Der Zant, H. S. J.; Rovira, C.; Burzurí, E.; Crivillers, N. Robust Organic Radical Molecular Junctions Using Acetylene Terminated Groups for C-Au Bond Formation. *J. Am. Chem. Soc.* **2018**, *140*, 1691–1696.
(30) Crivillers, N.; Paradinas, M.; Torrent, M. M.; Bromley, S. T.; Rovira, C.; Ocal, C.; Veciana, J. Negative Differential Resistance (NDR) in Similar Molecules with Distinct Redox Behaviour. *Chem. Commun.* **2011**, *47*, 4664–4666.

(31) De Sousa, J. A.; Bejarano, F.; Gutiérrez, D.; Leroux, Y. R.; Nowik-Boltyk, E. M.; Junghoefer, T.; Giangrisostomi, E.; Ovsyannikov, R.; Casu, M. B.; Veciana, J.; Mas-Torrent, M.; Fabre, B.; Rovira, C.; Crivillers, N. Exploiting the Versatile Alkyne-Based Chemistry for Expanding the Applications of a Stable Triphenylmethyl Organic Radical on Surfaces. *Chem. Sci.* **2020**, *11*, 516–524.
(32) Seitz, O.; Böcking, T.; Salomon, A.; Gooding, J. J.; Cahen, D. Importance of Monolayer Quality for Interpreting Current Transport through Organic Molecules: Alkyls on Oxide-Free Si. *Langmuir* **2006**, *22*, 6915–6922.
(33) Nerngchamnong, N.; Thompson, D.; Cao, L.; Yuan, L.; Jiang, L.; Roemer, M.; Nijhuis, C. A. Nonideal Electrochemical Behavior of Ferrocenyl-Alkanethiolate SAMs Maps the Microenvironment of the Redox Unit. *J. Phys. Chem. C* **2015**, *119*, 21978–21991.
(34) Bard, A. J.; Faulkner, L. R. *Electrochemical Methods; Fundamentals and Applications*; John Wiley & Sons, Ltd, **2002**.
(35) Carlotti, M.; Degen, M.; Zhang, Y.; Chiechi, R. C. Pronounced Environmental Effects on Injection Currents in EGaIn Tunneling Junctions Comprising Self-Assembled Monolayers. *J. Phys. Chem. C* **2016**, *120*, 20437–20445.
(36) Aviram, A.; Ratner, M. A. Molecular Rectifiers. *Chem. Phys. Lett.* **1974**, *29*, 277–283.
(37) Van Dyck, C.; Ratner, M. A. Molecular Rectifiers: A New Design Based on Asymmetric Anchoring Moieties. *Nano Lett.* **2015**, *15*, 1577–1584.
(38) Qiu, L.; Zhang, Y.; Krijger, T. L.; Qiu, X.; Hof, P. van t.; Hummelen, J. C.; Chiechi, R. C. Rectification of Current Responds to Incorporation of Fullerenes into Mixed-Monolayers of Alkanethiolates in Tunneling Junctions. *Chem. Sci.* **2017**, *8*, 2365–2372.
(39) Souto, M.; Yuan, L.; Morales, D. C.; Jiang, L.; Ratera, I.; Nijhuis, C. A.; Veciana, J. Tuning the Rectification Ratio by Changing the Electronic Nature (Open-Shell and Closed-Shell) in Donor-Acceptor Self-Assembled Monolayers. *J. Am. Chem. Soc.* **2017**, *139*, 4262–4265.
(40) Har-Lavan, R.; Yaffe, O.; Joshi, P.; Kazaz, R.; Cohen, H.; Cahen, D. Ambient Organic Molecular Passivation of Si Yields Near-Ideal, Schottky-Mott Limited, Junctions. *AIP Adv.* **2012**, *2*, 012164-012176.
(41) Salomon, A.; Berkovich, D.; Cahen, D. Molecular Modification of an Ionic Semiconductor-Metal Interface: ZnO/Molecule/Au Diodes. *Appl. Phys. Lett.* **2003**, *82*, 1051–1053.
(42) Riera-Galindo, S.; Chen, L.; Maglione, M. S.; Zhang, Q.; Bromley, S. T.; Rovira, C.; Mas-Torrent, M. Functionalising the Gate Dielectric of Organic Field-Effect Transistors with Self-Assembled Monolayers: Effect of Molecular Electronic Structure on Device Performance. *Appl. Phys. A Mater. Sci. Process.* **2022**, *128*, 1–7.
(43) Faber, E. J.; De Smet, L. C. P. M.; Olthuis, W.; Zuilhof, H.; Sudhölter, E. J. R.; Bergveld, P.; Van Den Berg, A. Si-C Linked Organic Monolayers on Crystalline Silicon Surfaces as Alternative Gate Insulators. *ChemPhysChem* **2005**, *6*, 2153–2166.
(44) Wimbush, K. S.; Fratila, R. M.; Wang, D.; Qi, D.; Liang, C.; Yuan, L.; Yakovlev, N.; Loh, K. P.; Reinhoudt, D. N.; Velders, A. H.; Nijhuis, C. Bias Induced Transition from an Ohmic to a Non-Ohmic Interface in Supramolecular Tunneling Junctions with Ga_2O_3/EGaIn Top Electrodes. *Nanoscale* **2014**, *6*, 11246–11258.
(45) Yakuphanoglu, F. Controlling of Silicon-Insulator-Metal Junction by Organic Semiconductor Polymer Thin Film. *Synth. Met.* **2010**, *160*, 1551–1555.
(46) Gupta, N. K.; Schultz, T.; Karuppannan, S. K.; Vilan, A.; Koch, N.; Nijhuis, C. A. The Energy Level Alignment of the Ferrocene-EGaIn Interface Studied with Photoelectron Spectroscopy. *Phys. Chem. Chem. Phys.* **2021**, *23*, 13458–13467.

(47) Trasatti, S. The Absolute Electrode Potential: An Explanatory Note. *Pure Appl. Chem.* **1986**, *58*, 955–966.
(48) Sze, S. M.; Ng, K. K. Physics of Semiconductor Devices. 3rd Edition.; John Wiley & Sons, Inc. **2006**.
(49) Rhoderick, E. H.; Williams, R. H. Metal-Semiconductor Contacts, 2nd Edition.; Oxford University Press. **1988**.
(50) Schroder, D. K. Material and Device Semiconductor Material and Device, 3rd Edition.; John Wiley & Sons, Inc. **2006**.
(51) Simmons, J. G. Generalized Formula for the Electric Tunnel Effect between Similar Electrodes Separated by a Thin Insulating Film. *J. Appl. Phys.* **1963**, *34*, 1793–1803.
(52) Salomon, A.; Boecking, T.; Seitz, O.; Markus, T.; Amy, F.; Chan, C.; Zhao, W.; Cahen, D.; Kahn, A. What Is the Barrier for Tunneling through Alkyl Monolayers? Results from n- And p-Si-Alkyl/Hg Junctions. *Adv. Mater.* **2007**, *19*, 445–450.
(53) Godet, C.; Fadjie-Djomkam, A. B.; Ababou-Girard, S.; Solal, F. Tunnel Barrier Parameters Derivation from Normalized Differential Conductance in Hg/Organic Monomolecular Layer-Si Junctions. *Appl. Phys. Lett.* **2010**, *97*, 13–16.
(54) Diez-Cabanes, V.; Seber, G.; Franco, C.; Bejarano, F.; Crivillers, N.; Mas-Torrent, M.; Veciana, J.; Rovira, C.; Cornil, J. Design of Perchlorotriphenylmethyl (PTM) Radical-Based Compounds for Optoelectronic Applications: The Role of Orbital Delocalization. *ChemPhysChem* **2018**, *19*, 2572–2578.
(55) Koster, L. J. A.; Mihailetchi, V. D.; Ramaker, R.; Blom, P. W. M. Light Intensity Dependence of Open-Circuit Voltage of Polymer:Fullerene Solar Cells. *Appl. Phys. Lett.* **2005**, *86*, 123509.
(56) Ocaya, R. O.; Al-Ghamdi, A.; Mensah-Darkwa, K.; Gupta, R. K.; Farooq, W.; Yakuphanoglu, F. Organic Photodetector with Coumarin-Adjustable Photocurrent. *Synth. Met.* **2016**, *213*, 65–72.
(57) Yakuphanoglu, F. Photovoltaic Properties of the Organic-Inorganic Photodiode Based on Polymer and Fullerene Blend for Optical Sensors. *Sensors Actuators, A Phys.* **2008**, *141*, 383–389.
(58) Zhang, Y.; Basel, T. P.; Gautam, B. R.; Yang, X.; Mascaro, D. J.; Liu, F.; Vardeny, Z. V. Spin-Enhanced Organic Bulk Heterojunction Photovoltaic Solar Cells. *Nat. Commun.* **2012**, *3*, 1043–1049.

Table of Contents (TOC)